STRUCTURAL CONTROL AND HEALTH MONITORING
Struct. Control Health Monit. 2008; **15**:797–820
Published online 8 July 2008 in Wiley InterScience
(www.interscience.wiley.com). DOI: 10.1002/stc.272

GA-optimized FLC-driven semi-active control for phase-II smart nonlinear base-isolated benchmark building

Sk. Faruque Ali[§] and Ananth Ramaswamy*[,†,‡]

Department of Civil Engineering, Indian Institute of Science, Bangalore 560 012, India

SUMMARY

An optimized fuzzy logic control (FLC) algorithm is developed for the phase-II smart base-isolated benchmark building with nonlinear isolation system. A restart genetic algorithm-based optimization strategy has been used to change the fuzzy system properties like the fuzzy rule base, pre-scale gains, membership function type and parameters at every simulation step. Acceleration and relative velocity responses at the damper location have been taken as inputs to the FLC system. Voltage required by the magneto-rheological (MR) damper is obtained as an output from the FLC. The use of MR dampers in the benchmark study as a control device along with isolation bearings in the building renders the overall system nonlinear. The advantage of using a fuzzy rule base is its inherent ability to handle nonlinearities and uncertainties in structural behavior, input excitation, sensor, and actuator dynamics. As a consequence, FLC provides robustness to the control mechanism. Moreover, FLC-driven MR damper voltage monitoring provides a gradual and smooth change of voltage. In the present study, the number of sensors and actuators and their locations have been kept unchanged as in the sample controller provided in the benchmark study. Simulation results for FLC, the adaptive rule and fixed rule base type, and results from the sample controller provided have been tabulated and compared. Results obtained indicate improvement using the proposed control approach without considering a multi-objective nondominated solution, where the weight of objective functions can be varied. A stability test for the proposed adaptive rule base FLC has been shown. Copyright © 2008 John Wiley & Sons, Ltd.

KEY WORDS: genetic algorithm; adaptive fuzzy logic controller; adaptive rule base design; benchmark building; nonlinear base isolation; semi-active vibration control

1. INTRODUCTION

Mitigation of structural damage induced by large loads, stemming from earthquake, is of particular interest to engineers. Specifically, seismic dominant regions provide a serious damage

*Correspondence to: Ananth Ramaswamy, Department of Civil Engineering, Indian Institute of Science, Bangalore-560 012, India.
[†]E-mail: ananth@civil.iisc.ernet.in
[‡]Associate professor.
[§]Research scholar.

Received 27 March 2007
Revised 1 April 2008
Accepted 8 April 2008

threat to both the infrastructure and human lives. Protection of civil structures, including its material content and the human occupants, is without doubt a priority to the designers worldwide. The extent of protection ranges from reliable operation and occupant comfort to human and structural survival.

Base isolation is the mostly used earthquake protective scheme for structures. Various researchers have studied the potential of base isolation and it has been practically implemented in many structures around the world [1]. However, serious damage can occur to a structure in cases of near-source excitations due to large motion of the base isolation devices. Therefore, the focus on protection of structures has moved from a base isolation mechanism to hybrid base isolation techniques, where base isolation is integrated with energy-dissipating devices such as hydraulic dampers [1]. Magneto-rheological (MR) dampers are a recent addition to this hybrid base isolation mechanism [2]. MR dampers operate on voltage provided externally. MR damper voltage should be monitored using a control algorithm to achieve the desired performance of the overall system.

The last decade has witnessed the idea of using external devices to control structural responses (accelerations, velocities, and displacements) as a means of hazard reduction [1,3]. The design philosophy is to reduce the structural responses under the limitation of both the control force level (limited by the number and actuator capacity and the required amount of energy to drive the system) and the number of measured signals. Various algorithms developed to operate these devices have been directly used to monitor the voltage of the MR damper. These approaches were used to provide optimal solution to linear systems, whereas the application of MR dampers introduces nonlinearity in the system. In addition, hardware-related constraints, such as saturation and resolution of the sensor, analog-to-digital converter, and digital-to-analog converter, lead to quantization errors. Recently, the applications of intelligent controllers [e.g. fuzzy logic controller (FLC), neural network controller, ANFIS, etc.] to the structural control problem have been studied extensively [4–12]. Some characteristics of intelligent systems appealing to control engineers are its effectiveness and ease in handling structural nonlinearities, uncertainties, and heuristic knowledge. The advantage of these techniques is that they are independent of structural models but rely on input–output data mapping. Vibration control using fuzzy logic, although studied earlier [6–8], is on the rise since recent times. There has been an increasing interest in applying FLC to structures [9–12] and some interesting results have been reported. Fuzzy control offers a simple and robust framework with which to specify nonlinear control laws and can accommodate uncertainties and imprecision in the system model. A major advantage of fuzzy control is that it requires only a linguistic description of the control law with fuzzy rules and does not require a detailed analytical description of the structure. Moreover fuzzy control can handle the hysteretic behavior of structures under earthquake [8]. Another advantage of the present FLC model in monitoring MR damper voltage is that unlike clipped optimal and Lyapunov control techniques, the change in voltage input to the MR damper is gradual and it covers all voltage values in the range of maximum and minimum damper voltage [0,1]. This particular advantage not only permits the designer to use any voltage value between [0,1] but also provides an inherent stability to the closed-loop system [13]. From the stability point of view the FLC-driven MR damper brings structural responses to rest in a short time in comparison with the Lyapunov control-driven MR damper as shown later in this study.

It has been observed that the major drawback of most fuzzy controller systems is the need to predefine membership functions (MFs) and fuzzy rules. The fuzzy sets and rules that require

DOI: 10.1002/stc

a full understanding of the system dynamics must be correctly pre-determined for a system to function properly. This needs a complete understanding of the mechanics of the system. Furthermore, it becomes more critical to design FLC manually, while reducing the responses of a seismically excited civil engineering structure with multiple MR dampers distributed throughout the structure. A natural evolution is to integrate genetic algorithms (GAs) into the fuzzy logic design process. The automatic definition of a fuzzy rule-based system can be seen as an optimization or search problem, and GAs are a well-known and widely used global search technique with the ability to explore a large search space for suitable solutions only requiring a performance measure. The development of these techniques to design optimal robust FLCs, for example, automotive active suspension system [14], aerospace autopilots [15] to structural vibration control under earthquake excitation [16–18], has arisen to satisfy the need that exists when expert heuristic knowledge is not available for translation into the controller design. In the present study two different micro-genetic algorithm (GA)-optimized FLCs have been explored. The optimization of the FLC parameters has been carried at every simulation time step online. In this study, the FLC receives acceleration and relative velocity of the structure at the damper location as input variables and provides the required MR damper voltage to drive the controller as the output. Input scaling gains for both the inputs have been optimized along with the rule base, MF type, and parameter. The optimization algorithm selects either *trapezoidal* or *triangular* functions as a membership base by altering the parameters. The initial rule base consisting of 25 rules have been selected based on the fundamental mode of vibration of a single degree-of-freedom system [9,10]. The rule base has been modified based on a newly developed method [19]. The modification of FLC rule base at every simulation step based on the feedback from the system to satisfy the pre-defined cost function is defined here as adaptive in the present study. In the study a geometric approach has been evolved to account for the symmetry in a rule base and input–output relationship (detailed in a later section).

The proposed method has been implemented on the recently developed nonlinear base-isolated benchmark building problem proposed by Nagarajaiah *et al.* [20] and Narashiman *et al.* [21] discussed in the ensuing section. The stability of the algorithm against change in the mass and the amplitude of earthquake has also been shown.

2. BENCHMARK BUILDING PROBLEM DEFINITION

The benchmark structure is an L-shaped nonlinear base-isolated eight-story, steel-braced framed building, 82.4 m long and 54.3 m wide, similar to an existing building in Los Angeles, CA [20–22]. The isolators are connected between the superstructure and the footings below at the column locations. Further details of the problem definition can be found in [20–24].

Base-isolated buildings are designed such that the superstructure remains elastic. Hence, the superstructure is modeled as a three-dimensional linear elastic shear building. In addition, the localized nonlinearities at the isolation level allow condensation of the linear superstructure. Each nonlinear isolation bearing or device is modeled explicitly using the discrete biaxial Bouc-Wen model, and the forces in the bearings or devices are transformed to the center of mass of the base using a rigid base slab assumption. All the linear isolation bearings or devices can be modeled individually or globally by equivalent lumped elements at the center of mass of the base. The equations of motion for the elastic superstructure are expressed in the

DOI: 10.1002/stc

following form:

$$\mathbf{M}_{n\times n}\ddot{\mathbf{U}}_{n\times 1}+\mathbf{C}_{n\times n}\dot{\mathbf{U}}_{n\times 1}+\mathbf{K}_{n\times n}\mathbf{U}_{n\times 1}=-\mathbf{M}_{n\times n}\mathbf{R}_{n\times 3}(\ddot{\mathbf{U}}_{\mathrm{g}}+\ddot{\mathbf{U}}_{\mathrm{b}})_{3\times 1} \tag{1}$$

where n is three times the number of floors (excluding the base), $\mathbf{M}$ is the superstructure mass matrix, $\mathbf{C}$ (modal damping ration = 5%) and $\mathbf{K}$ are the superstructure damping and stiffness matrices, respectively, in the fixed-base case, and $\mathbf{R}$ is the matrix of earthquake influence coefficients. Furthermore, $\ddot{\mathbf{U}}$, $\dot{\mathbf{U}}$, and $\mathbf{U}$ represent the floor acceleration, velocity, and displacement vectors relative to the base, respectively; $\ddot{\mathbf{U}}_{\mathrm{b}}$ is the vector of base accelerations (at the isolation level) relative to the ground and $\ddot{\mathbf{U}}_{\mathrm{g}}$ is the vector of ground accelerations. The equations of motion for the base are as follows:

$$\mathbf{R}^{T}_{3\times n}\mathbf{M}_{n\times n}[\ddot{\mathbf{U}}_{n\times 1}+\mathbf{R}_{n\times 3}(\ddot{\mathbf{U}}_{\mathrm{g}}+\ddot{\mathbf{U}}_{\mathrm{b}})_{3\times 1}]_{n\times 1}+\mathbf{M}_{\mathrm{b}_{3\times 3}}(\ddot{\mathbf{U}}_{\mathrm{g}}+\ddot{\mathbf{U}}_{\mathrm{b}})_{3\times 1}+\mathbf{C}_{\mathrm{b}_{3\times 3}}\dot{\mathbf{U}}_{\mathrm{b}_{3\times 1}}$$
$$+\mathbf{K}_{\mathrm{b}_{3\times 3}}\mathbf{U}_{\mathrm{b}_{3\times 1}}+\mathbf{f}_{3\times 1}=0 \tag{2}$$

in which $\mathbf{M}_{\mathrm{b}}$ is the diagonal mass matrix of the rigid base, $\mathbf{C}_{\mathrm{b}}$ is the resultant damping matrix of viscous isolation elements, $\mathbf{K}_{\mathrm{b}}$ is the resultant stiffness matrix of elastic isolation elements, and $\mathbf{f}$ is the vector containing the nonlinear bearing forces, device forces, and control forces.

2.1. Evaluation criteria

The benchmark problem [20] defines a set of nine evaluation criteria to evaluate the capabilities of each proposed control strategy. The performance indices are shown in Table I, and more details can be found in [20–24]. The indices J_1–J_5 measure the peak values of the base shear (V_0), structural shear (V_1), base displacement (x_{b}), inter-story drift (d_f), and floor accelerations (a_f), respectively. These values are normalized by their respective uncontrolled values (represented by ($\hat{}$)); 'uncontrolled' refers to the case when there is no force feedback to the structure and the control devices are disconnected from the structural system (i.e. the building with the isolation bearing). The performance index J_6 measures the maximum control force (f_d) developed in the device normalized by the peak base shear. The indices, J_7 and J_8, measure the RMS values of the base displacement (σ_d) and the base acceleration (σ_a), respectively, normalized by their uncontrolled values. The index J_9 measures the energy dissipated by the semi-active device as a percentage of the input excitation energy. In Table I f denotes the floor number ($1\cdots 8$), $\langle\cdot\rangle$ denotes the inner product, and $\|\cdot\|$ means the vector norm. The performance indices are to be simulated for a set of near-fault earthquake excitations ($\ddot{U}_{\mathrm{g}}$). The earthquake excitations used in the benchmark study are

Table I. Performance indices.

Peak base shear	Peak structure shear	Peak base displacement
$J_1=\frac{t_{\max}\|V_0(t)\|}{t_{\max}\|\hat{V}_0(t)\|}$	$J_2=\frac{t_{\max}\|V_1(t)\|}{t_{\max}\|\hat{V}_1(t)\|}$	$J_3=\frac{t_{\max}\|x_{\mathrm{b}}(t)\|}{t_{\max}\|\hat{x}_{\mathrm{b}}(t)\|}$
Peak interstory drift	Peak floor acceleration	Peak control force
$J_4=\frac{t,f_{\max}\|d_f(t)\|}{t,f_{\max}\|\hat{d}_f(t)\|}$	$J_5=\frac{t,f_{\max}\|a_f(t)\|}{t,f_{\max}\|\hat{a}_f(t)\|}$	$J_6=\frac{t_{\max}\|f_d(t)\|}{t_{\max}\|V_0(t)\|}$
RMS base displacement	RMS floor acceleration	Energy dissipated by devices
$J_7=\frac{i_{\max}\|\sigma_d(t)\|}{i_{\max}\|\sigma_{\hat{d}}(t)\|}$	$J_8=\frac{f_{\max}\|\sigma_a(t)\|}{f_{\max}\|\sigma_{\hat{a}}(t)\|}$	$J_9=\frac{[\int_0^{\mathrm{T}} f_d(t)\ \dot{x}_{\mathrm{b}}(t)\,\mathrm{d}t]}{\int_0^T\langle V_0(t)\ \dot{U}_{\mathrm{g}}(t)\rangle\,\mathrm{d}t}$

DOI: 10.1002/stc

Newhall, Sylmar, El-Centro, Rinaldi, Kobe, Jiji, and Erzinkan. Earthquake records have been considered in both fault-parallel (FP) and fault-normal (FN) directions.

3. FLC DESIGN

The performance of conventional controllers (Pole placement, LQR, etc.) depends fully on the accuracy in the modeling of the system dynamics and is effective in controlling the linear structural behavior. Complex structural systems possess nonlinearities and uncertainties in the structural properties and measurements. Consequently, standard analytical model-based control techniques are impractical. As an alternative to the conventional control theory, FLC allows the resolution of imprecise or uncertain information. FLC can also map the nonlinear input–output relationship effectively and easily. Moreover, fuzzy control can handle the hysteretic behavior of structures under earthquake loads [8]. In civil engineering, the fuzzy set theory has been applied by Joghataie and Ghaboussi [6], Subramaniam *et al.* [7], Battaini *et al.* [8], Ahlawat and Ramaswamy [10–12,25], etc.

FLC is a simulation of logical reasoning of the human brain; it maps an input space to a corresponding output space based on fuzzy rules specified in if–then format known as the knowledge base. Fuzzy logic-based control includes a fuzzification interface, an inference engine, and a defuzzification interface as shown in Figure 1. The following steps provide a simple design for the FLC.

- *Defining input, output variables*: A decision on what responses of the system are subject to observation and measurement, leading to choice as input variables, is the first step. The choice of control functions needed results in the choice of output variables. In the examples provided, relative velocity and absolute acceleration data have been considered to be input variables and the MR damper voltage as an output variable. We have chosen relative velocity and acceleration as two input variables as they are out-of-phase variables for a system.
- *Fuzzification of input variables*: The fuzzification interface maps the measurable input variables in the form of a crisp set to a fuzzy linguistic value based on their membership grade in the domain of discourse [26]. Usually, within a domain of discourse the number of partitions for linguistic variables should be odd in number. This number will decide the status of a partition of the space. The more the linguistic variables, the more sophisticated is the partition of spaces but it increases the computational cost. In the present FLC control, five trapezoidal MFs have been taken to cover the input and output domains. Trapezoidal MFs can be changed to triangular MFs based on optimization by a GA.

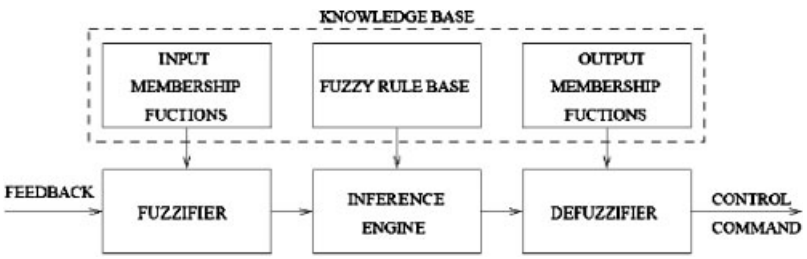

Figure 1. General structure for fuzzy logic controller design.

DOI: 10.1002/stc

		Acceleration				
Velocity		**PL**	**PS**	**ZE**	**NS**	**NL**
	PL	PL	PL	PS	PS	ZE
	PS	PL	PS	PS	ZE	NS
	ZE	PS	PS	ZE	NS	NS
	NS	PS	ZE	NS	NS	NS
	NL	ZE	NS	NS	NS	NL

Figure 2. Inference rules for fixed rule base FLC.

- *Inference engine*: The inference engine has a dual role in the fuzzy control theory. It maps the input fuzzified variables to the output variables based on user-defined rules known as the knowledge base. It also provides a decision based on the results obtained from implementation of these rules. Mamdani's MAX–MIN operator is the most commonly used inference scheme [26] and has been adopted for the present study.

Usually, the control rule base of the fuzzy controller is formed from operator experience and expert knowledge. The more the control rules, the more the efficiency of the control system. Control rules are usually in the form of if–then rules to link input and output variables. 'if' is called antecedent; 'then' is called consequence.

For example, rule R_i : If *velocity* is *positive large* and *acceleration* is *positive large*, then *control voltage* is *positive large*; $i = 1, \ldots, n$, where n represents the number of control rules. The initial FLC rule base adopted in this study (which is modified based on optimization) is shown in Figure 2.

- *Defuzzification of output variables*: Defuzzification describes the mapping from the space of fuzzy outputs to a crisp set output. The defuzzification operation takes most of the processing time in a fuzzy control algorithm. A large number of defuzzification methods are available but only few are practically amenable for fuzzy control systems. They are center of area, center of gravity, center of largest area, mean of the maximum, etc. In this paper the COA defuzzification algorithm (MATLAB® [27]) has been used.

4. GA-BASED OPTIMAL FLC

The design of an optimal FLC can be viewed as a search in a multi-dimensional space or hypersurface, where combinations of differing component properties of the fuzzy system (rule base, input–output MFs, their properties, and scaling gains) correspond to a point in that space.

DOI: 10.1002/stc

Fuzzy search surfaces are large, since the choice in the number and properties of fuzzy sets for each variable is unlimited, nondifferentiable as changes in fuzzy set numbers and rules are discrete and therefore create points of discontinuity on the surface and multi-modal, since different rule bases and MFs may have comparable performance [25].

These characteristics of FLC make the application of a GA to find an optimal location within the search surface feasible and attractive. Genetic learning of a fuzzy system involves a process of automatically generating from scratch all properties of rule bases, MFs, or both, with no prior knowledge in respect of either or both in order to optimize the FLC response [28]. In this study, an online optimization of the FLC has been attempted with *a priori* information in relation to the number of rules and the number of MFs that give meaning to those rules. A number of approaches have been studied and reported in the literature [28,29] like the Michigan technique, the iterative rule techniques, the Pittsburgh approach, etc. The literature [28] contends that the Pittsburgh method of FLC optimization is preferable as structuring the GA population in this way induces, through increased competition, better cooperation among the rules with respect to the FLC performance. The main drawback of the Pittsburgh approach, however, is that it is computationally more demanding as the required chromosome size is greater, thus increasing the search space and therefore not being suitable for online simulation (simulation at every time step). A newly developed method similar to the Pittsburgh approach, reported in [19], has been adopted in the present paper with modification to suit the problem. For the GA used in this study, each chromosome represents a complete FLC as defined by MATLAB® [27] fuzzy inference files (FIS) and, hence, is consistent with the Pittsburgh approach but the method minimizes on the chromosome size (at most 44 bits used) making it suitable for online optimization. Figure 3 illustrates the 44 strings of binary GA chromosome used to encode each FLC. First 1–9 binary strings have been set to modify the rule base, next 2277×3 strings code the input–output MF type and parameter. The remaining 14 bits have been used to code the input scaling gains.

The paper compares two different micro-GA-optimized FLCs: (i) optimization scheme where only the MF type, parameters, and pre-scaling gains are modified at every simulation time step (i.e. real time) keeping the rule base fixed (henceforth, we call it fixed rule base (FRB)–FLC), and (ii) optimization scheme where the MF type, parameters, pre-scaling gains along with the rule base are optimized (henceforth, we call it adaptive rule base (ARB)–FLC) at every simulation time step. In ARB–FLC three aspects of the knowledge base (see Figure 1) have been subjected to optimization. ARB–FLC uses all 44 strings for its optimization and for FRB–FLC, 35 (*the first* 9 *are constant*) binary strings have been used. ARB–FLC needs an initial rule base, which it modifies to satisfy the objective function. The FLC input–output relation in the first mode of vibration of the structure [9,10] has been exploited to design the initial ARB keeping the symmetry in the rule base intact. To achieve the symmetry in rule base, a geometric approach is taken, which reduces the required chromosome length, and thereby the search space is reduced. This reduces the computational overhead of the optimization scheme. The choice of

Rule Base (1:9)	MF Velocity (10:16)	MF Accel (17:23)	MF Control (24:30)	Scaling Velocity (31:37)	Scaling Accel (38:44)

Figure 3. GA chromosome structure to optimize ARB–FLC (rule base is not there in FRB–FLC).

DOI: 10.1002/stc

the initial rule base pattern is dependent on the first mode of vibration of the structure; in effect it represents an *a priori* knowledge being made available to the algorithm (see Figure 2).

4.1. ARB design

In this study the FLC has two inputs (premises), relative velocity and acceleration at the point of the action of the damper and one output (consequent), control voltage, $u(t) \in [0, 1]$, which is then passed to the *MRDAMPER.dll* file provided with the benchmark study. The input variables have been normalized over the UOD (universe of discourse) of $[-1, 1]227$. All FLC variables range their respective UOD using five MFs (NL = negative large, NS = negative small, ZE = zero, PS = positive small, PL = positive large). It is to be noted that the output also contains five MFs and ranges $[-1, 1]227$; this has been done to keep the symmetry about zero in the UOD. Therefore, to get the output voltage as positive values between [0,1], the MATLAB® *abs* function has been used. The following assumptions have been considered while designing the rule base:

- The magnitude of the output control action is consistent with the magnitude of the input values, (i.e. in general, extreme input values (premise) result in extreme output values (consequent), mid-range input values result in mid-range output values, and small/zero input values result in small/zero output values) [9,10]. This rule base pattern is based on the first mode of vibration of structures. Since the base-isolated structure acts as a single degree-of-freedom system, the assumption is rational.
- If a large negative/positive input generates a large positive control output [$u(t)$[0, 1]], then it is likely that slightly smaller, negative/positive inputs will necessitate a response of smaller magnitude, and so forth. A situation may arise where the displacement of the structure keeps increasing at small rate or constant displacement, which results in negligible/zero velocity and acceleration. In such a situation the FLC will provide a zero voltage output and the structure displacements will be taken care by the MR damper acting as a passive device.

In this geometric approach the consequent space is overlayed upon the 'premise coordinate system' and is in effect partitioned into nonoverlapping small regions (in our case 5), where each region represents a consequent fuzzy set (see Figure 4). To design the ARB we define a consequent line as shown in Figure 4. The line is made pivotal on premise zero–zero position (i.e. both inputs being zero) and it is free to rotate over the consequent space and therefore the rule base adapts according to the optimization scheme. It is to be noted that the rule base remains symmetrical whatever be the position of the consequent line. The rule base is then extracted by determining the consequent region in which each premise combination point lies. The geometric approach is made possible using two parameters.

- Slope of the consequent line angle (CA): It has been used to create the output space partitions (angles between 0 and 180), as the output $u(t)$ range is [0, 1].
- Consequent-region spacing (CS): As shown in Figure 4 a proportion of the fixed distance between the premises (NS, NL, ZE, PS, PL) on the coordinate system is used to define the distance between consequent points along the consequent line. This is taken as (0.5 *to* 1.5) × PS, where PS is the corresponding distance obtained in an FRB case (see Figure 2).

Thus, only two variables are needed to be encoded for optimization of the rule base. Assuming the consequent line angle to be 45° and the consequent-region spacing to be 1, we get

DOI: 10.1002/stc

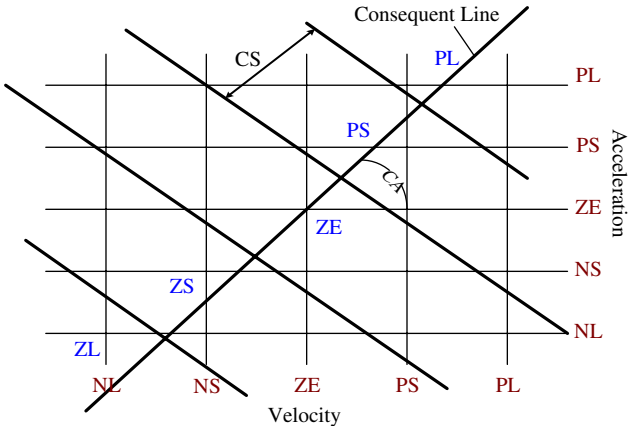

Figure 4. Adaptive rule base design for FLC.

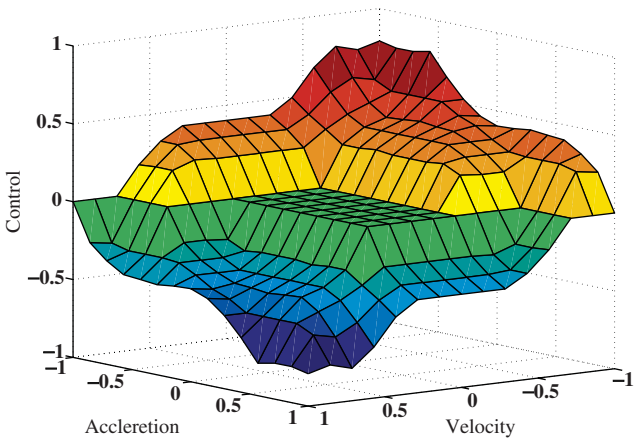

Figure 5. FLC input/output surface [Kobe EQ (FP-X, FN-Y)].

a rule base analogous to the rule base that can be derived from the first mode vibration of the structure. This rule base has been used later in the paper for simulation of the system with a FRB (see Figure 2). Figure 5 shows one such input–output surface obtained in ARB–FLC optimization at the end of the simulation.

4.2. Adaptive MF design

The MF properties altered by the GA are MF shape (*triangular* or *trapezoidal*), MF center shift and MF concentration, or dilation [12,29]. While attempting to encode the FLC MFs associated with the two inputs and one output, the UOD is kept symmetrical about the central, zero region for each variable. The extreme MF for input variables are kept unbounded in the respective positive (s-shaped) and negative (z-shaped) UOD [12]. The output variable extreme MFs could

DOI: 10.1002/stc

assume the same shape as inner and central MFs (either *triangular* or *trapezoidal*). In addition, the algorithm uses the offset value to ensure that 50% overlap is maintained between adjacent MFs. The apex for (*triangular*) or the plateau for (*trapezoidal*) MFs is only coincident with zero-valued segments of other adjacent and nonadjacent MFs within the UOD. Further, to enable evaluation of nonuniform distributed MFs, concentration or dilation of the associated MFs is also encoded. This is achieved by raising each of the MF to the power of [0.5, 2]. Figure 6 shows two inputs and one output MF type and distribution obtained in the optimization of ARB–FLC. It should be observed that all the constraints stated above are satisfied and there is a mixture of *triangular*- and *trapezoidal*-type MFs for a variable.

4.3. Restart GA

Restart GA (popularly known as micro-GA) was proposed by Krishnakumar [30] and Goldberg [31] to improve the performance of the GA at lower population sizes. The micro-GA operates on a family, or population, of designs similar to the Simple Genetic Algorithm (SGA) but with a lower population size. The basic idea is to use a smaller population GA and allow it to converge rapidly and invoke random population and start the search again (i.e. restart the GA) keeping

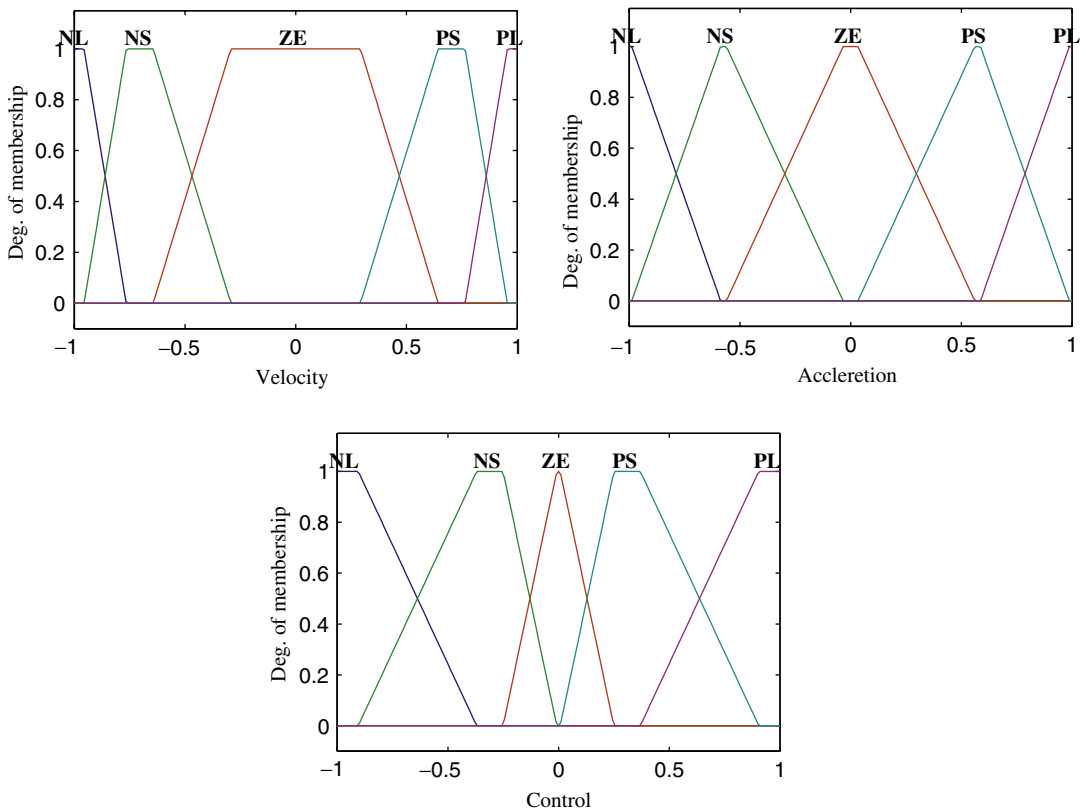

Figure 6. Sample input/output MFs [Kobe EQ (FP-X, FN-Y)].

DOI: 10.1002/stc

the elitist chromosome unchanged. Restart GA performs better in multi-modal optimization problems and is therefore suitable for the FLC optimization. To restart the GA search the current population has been aggressively mutated. In addition, Krishnakumar [30] has shown that micro-GAs reach the optimum in fewer function evaluations compared with an SGA. This makes the application of the micro-GA suitable for online applications and parallel processing [32].

In this study, micro-GAs with the following specifications have been used.

1. The initial population search space is sub-divided into two complimentary subspaces. Half of the initial population is selected randomly and the other half is obtained by taking compliment of the initial half. In this manner any localization of the initial population is minimized. It has been reported in [30] that even as few as a five-member population can provide a global convergence. Here, we use an initial population size of 20 and the maximum number of generation has been selected as 50. Restart has been initiated when all members in the population have been observed to attain same fitness.
2. Gray encoding and decoding are used [33].

   Ordinary binary value representation in GA may sometimes be trapped in inefficient crossover [33] [i.e. offsprings result in lesser fitness value than parents]. The gray code avoids this problem by redefining the binary numbers such that the consecutive numbers have a Hamming distance of 1. The gray code is obtained by passing every consecutive binary number through an XOR operation.
3. Proportional fitness with stochastic universal sampling (SUS) is used [33–35]. SUS is markedly different from the Roulette Wheel selection technique. It is best described as a multi-pointer Roulette Wheel selection technique. In this method n (number of individuals in intermediate group) points are selected in the fitness line with the first one chosen randomly and others made equidistant from the previous one. Fitness values (a fitness function is a numeric value returned by the cost function as given in Equation (3)) of individuals within these points are selected. Individuals having higher fitness are given a higher share of fitness line (as in the Roulette Wheel) and therefore have a greater chance of selection. Since, SUS selects individuals in a single turn it is faster and efficient than the Roulette Wheel selection.
4. A two-point cross-over with a probability of 0.4 is considered.
5. A mutation probability of 0.01 is taken for all iterations, and a value of 0.5 is taken at the time of restart.

A simple GA requires intensive computation for online FLC optimization on a PC. A hardware implementation of the GA using reprogrammable field-programmable gate arrays (FPGA) decreases the computational time by 2–3 orders of its time in a simple PC [36]. These are problem and model specific. A flexible GA chip, which can dynamically perform various fitness function computations, four different cross-over operations, and over a thousand different types of mutation operations, has been developed by Chen *et al.* [37]. Real-time applications of GA-FLC using FPGA and fuzzy chips have been reported widely from a laboratory-scaled power system and an automotive active suspension system to structural control [14,38–40].

Hailin and Dongming [41] reported an adaptive fuzzy controller optimized by hardware-based GA (FPGA) and applied it to the feedback control of an inverted pendulum with

DOI: 10.1002/stc

a chromosome length of 32 bits and a population of 32 members. It has been reported that the proposed hardware GA processor is effective and efficient to solve optimal control problems. The reported processor can complete optimization within 26.5 ms, which is faster than C language software computation by a magnitude three. The optimization method proposed in the present paper using restart GA is computationally more efficient than simple GA and is therefore suitable for real-time FLC optimization. Therefore, hardware GA combining with a fuzzy control chip should have a wide application in the field of real-time control systems and can implement the present simulations realistically.

5. NUMERICAL SIMULATION AND RESULTS

The simulation starts with the loading of the initial rule base as shown in Figure 2 to the *Simulink*® [27] model (Figure 7). Two different fuzzy models have been used in two orthogonal directions, i.e. one genetically optimized FLC has been used for all controllers in the *X*-direction and another GA-optimized FLC for all controllers in the *Y*-direction. This has been done to save computational overhead. For a real-time application the optimization algorithm can be burnt into a chip [25,42]. Since the uncontrolled (base-isolated structure without controllers) dynamics show a similar nature of vibration at all sensors in a particular direction, the rule base used for that direction could be the same. In this case only the scaling factor changes, which should be different for different sensor data. Therefore, the present optimization technique provides a scaling factor optimal for all sensor data in one direction. Each evaluation of GA uses a 'genetically altered' version of the original FLC, which is defined using a MATLAB® *FIS* structure [27]. In the present study, the number of sensors and actuators are kept same as in the benchmark exercise. The FLC output [$u(t)$] is the voltage input to the MR damper and therefore $u(t)$ has been kept within the range [0, 1]227. Since FLC output can take any value in the range [0, 1]227, it can smoothly change the voltage required for the MR damper and does not switch between the maximum and minimum value of the MR damper voltage range [13].

Base isolations are provided to separate the superstructure from catastrophic earthquake excitations. However, the excessive displacement that the isolators undergo in near-fault ground motion is a cause of concern for the structural engineers [2]. Nonlinear passive dampers are provided to limit the bearing displacement in such situations. This, however, increases the forces in the superstructure and at the isolation level. In the present study MR dampers are provided to minimize bearing displacement as well as to keep the structure and isolation-level shear forces at minimum. The FLC has been optimized at every simulation time step using GA to meet this demand, i.e. minimize bearing displacement (normalized w.r.t. uncontrolled bearing displacement) while maintaining the magnitude of the base shear and floor acceleration to be not more than the corresponding values for the no-damper simulation. Absolute values (|.|) are taken to minimize the maximum values irrespective of the direction of the motion. Therefore, the weighted multi-objective function to be optimized by GA is taken to be

$$\phi_1 = w_1\left(\frac{|V_0(t)|}{|\hat{V}_0(t)|} - 1\right) + w_2\left(\frac{|x_b(t)|}{|\hat{x}_b(t)|}\right) + w_3\left(\frac{f_{\max}|a_f(t)|}{f_{\max}|\hat{a}_f(t)| - 1}\right) \tag{3}$$

where w_i's are the weights for each objective. By suitably adjusting the weights a set of nondominated pareto optimal solutions can be obtained. For an online application one has to

DOI: 10.1002/stc

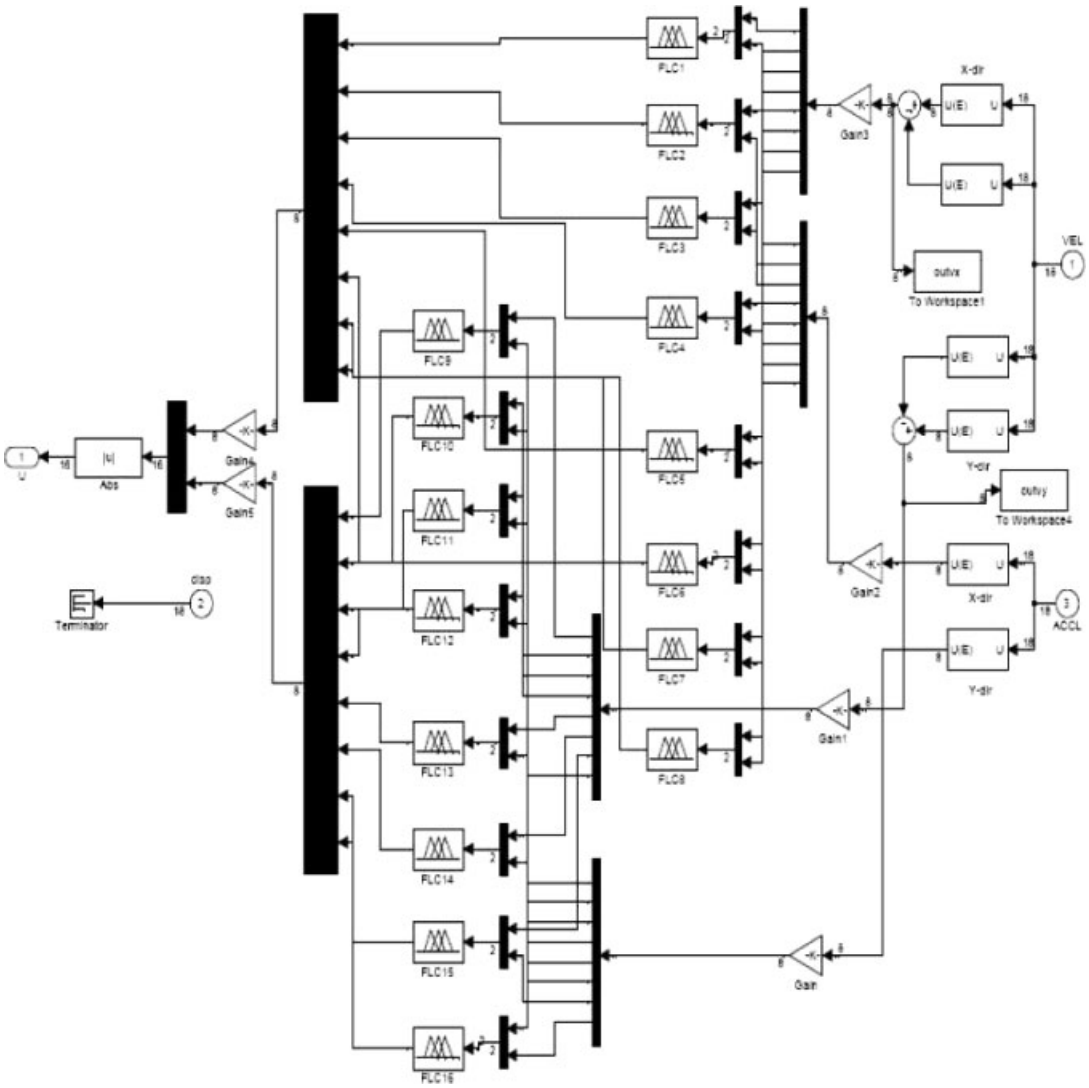

Figure 7. FLC Simulink block.

choose one such nondominated solution. In the present analysis $w_1 = w_3 = 1.0$ and $w_2 = 4.0$ (user choice), i.e. higher importance to bearing displacement has been reported. $V_0(t)$, $x_b(t)$, $a_f(t)$, and their corresponding () variables are described in Table I and in Section 2.1.

This paper presents a comparison between genetically optimized FLC where the rule base has been kept unaltered, which we call the fixed rule base FLC (FRB–FLC) and the genetically optimized adaptive rule base FLC, which we summon as the adaptive rule base FLC (ARB–FLC). In both the cases, optimization has been performed online, i.e. at every simulation time step. In FRB–FLC, GA optimizes the scaling factor for inputs and MF type and

DOI: 10.1002/stc

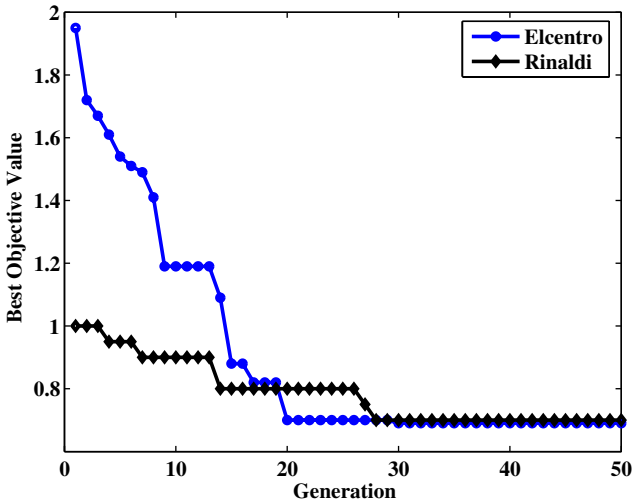

Figure 8. Convergence of GA: best objective value.

Table II. Performance indices, peak values (fault parallel (FP)-X and fault normal (FN)-Y).

PI	Control	Newhall	Sylmar	El-Centro	Rinaldi	Kobe	Jiji	Erzinkan
J_1	Lyapunov	1.0200	0.9900	1.2800	0.9500	1.1200	0.8500	0.9800
	FRB–FLC	1.0916	1.0080	1.0852	1.1225	1.0936	0.9082	1.0729
	ARB–FLC	1.0122	0.9208	1.2490	0.9290	1.0708	0.8391	1.0034
J_2	Lyapunov	0.9300	1.0200	1.2100	0.9200	1.2600	0.8600	0.9900
	FRB–FLC	1.0830	1.0089	1.1281	1.2067	1.1556	0.9194	1.0987
	ARB–FLC	0.9520	0.9100	1.2231	0.9412	1.3998	0.8306	1.0082
J_3	Lyapunov	0.7000	0.7500	0.4800	0.8000	0.6100	0.7200	0.7000
	FRB–FLC	0.8410	0.7727	0.7328	0.8301	0.7394	0.6993	0.7242
	ARB–FLC	0.6877	0.8021	0.4422	0.7906	0.5898	0.4596	0.6420
J_4	Lyapunov	1.2000	1.1300	1.2400	1.0200	1.3700	0.9500	1.0300
	FRB–FLC	1.0790	0.9228	1.0412	1.1879	1.1440	0.8563	1.0053
	ARB–FLC	1.2034	0.9412	1.2446	1.0003	1.4212	0.8404	1.0545
J_5	Lyapunov	1.1600	1.5600	1.2600	1.7300	1.5600	1.3000	1.4000
	FRB–FLC	1.2564	1.2176	1.1603	1.5366	1.2487	0.9406	1.2506
	ARB–FLC	1.1565	1.0710	1.1004	1.4821	1.5817	1.0507	1.3549
J_6	Lyapunov	0.2900	0.2400	0.4300	0.2700	0.3200	0.1700	0.2600
	FRB–FLC	0.2678	0.2805	0.3686	0.2953	0.3267	0.4310	0.2976
	ARB–FLC	0.2419	0.2103	0.4074	0.2639	0.3358	0.3864	0.2528

parameters [9], whereas in ARB–FLC, the GA is used to optimize the initial rule base of the FLC along with the scaling factor and MF type and parameter.

Simulations with an online automatic selection of optimal FLC parameters have been run for all given earthquake time histories in both FP and FN directions with FRB–FLC and ARB–FLC to minimize the optimization cost function (Equation (3)). The convergence of the GA with generation is shown in Figure 8 obtained in El-Centro and Rinaldi earthquakes after 1 s of simulation run.

DOI: 10.1002/stc

Table III. Performance indices, RMS values (FP-X and FN-Y).

PI	Control	Newhall	Sylmar	El-Centro	Rinaldi	Kobe	Jiji	Erzinkan
J_7	Lyapunov	0.5600	0.5800	1.0500	0.7500	0.6500	0.7100	0.6100
	FRB–FLC	0.9132	0.8037	0.9549	0.8731	0.8664	0.7536	0.8047
	ARB–FLC	0.5805	0.6490	0.9268	0.6979	0.5857	0.4218	0.5161
J_8	Lyapunov	1.3600	1.3300	1.3700	1.5300	1.3800	1.6100	1.1200
	FRB–FLC	1.3709	1.2370	1.3530	1.4359	1.4000	1.3275	1.1340
	ARB–FLC	1.3523	1.0241	1.3401	1.4366	1.4082	1.7953	1.0694
J_9	Lyapunov	0.4400	0.4700	0.4300	0.4400	0.4300	0.3300	0.4800
	FRB–FLC	0.4996	0.3495	0.3344	0.4382	0.4896	0.4478	0.4040
	ARB–FLC	0.4093	0.2580	0.2406	0.4171	0.3781	0.4687	0.4402

Table IV. Performance indices, peak values (FN-X and FP-Y).

PI	Control	Nehall	Sylmar	El-Centro	Rinaldi	Kobe	Jiji	Erzinkan
J_1	Lyapunov	1.0200	1.0000	1.4400	0.9200	1.1800	0.8600	1.0100
	FRB–FLC	1.0985	1.0167	1.5281	1.1154	0.9878	0.9008	1.0882
	ARB–FLC	1.0219	0.9905	1.4278	1.0453	1.1964	0.8004	1.0441
J_2	Lyapunov	0.8900	1.0400	1.2400	0.8800	1.1400	0.8700	0.9900
	FRB–FLC	1.0439	0.9472	1.3065	1.1011	0.9902	0.8153	0.9604
	ARB–FLC	0.9487	1.0037	1.4646	1.0220	1.3711	0.8122	0.9945
J_3	Lyapunov	0.7200	0.7900	0.7700	0.7600	0.5500	0.7100	0.5900
	FRB–FLC	0.8672	0.7835	0.8213	0.8330	0.7738	0.7500	0.6719
	ARB–FLC	0.6817	0.8109	0.5429	0.7510	0.5910	0.6373	0.6002
J_4	Lyapunov	1.1100	0.9200	1.2000	0.9300	1.3900	0.9000	1.0400
	FRB–FLC	1.1451	0.8963	1.1559	1.1868	1.0890	0.7998	0.9996
	ARB–FLC	1.3086	0.8767	1.4868	1.0523	1.4934	0.8501	1.0559
J_5	Lyapunov	1.2800	1.6200	1.2900	1.3400	1.5300	0.9500	1.5600
	FRB–FLC	1.2523	1.2320	1.2413	1.4502	1.4963	0.9016	1.0306
	ARB–FLC	1.5201	1.3236	1.3865	1.3959	1.4416	0.9369	1.0708
J_6	Lyapunov	0.2900	0.2300	0.4000	0.3000	0.3100	0.1700	0.2500
	FRB–FLC	0.2210	0.2238	0.3985	0.2292	0.4225	0.1745	0.2237
	ARB–FLC	0.2504	0.1553	0.3813	0.2498	0.3759	0.1814	0.2370

Results have been tabulated for both FRB–FLC and ARB–FLC along with the results from the sample controller as shown in Tables II–V. Tables II and IV show the peak values of the performance criteria, whereas Tables III and V show the RMS values of the performance criteria. The performance function results for both the proposed cases, fixed and adaptive FLC, are seen to be comparable to the corresponding values reported for the sample controller. In this example the objective has been the minimization of base displacement and from Tables II and IV it can be noticed that the row containing J_3 has the minimum for the ARB–FLC. Almost all performance indices for the ARB–FLC are found to be better than the sample controller provided with the benchmark exercise. In some cases [e.g. Jiji (FP-X FN-Y) and El-Centro (FN-X FP-Y) earthquakes] the decrease in base displacement has been found to be 0.6–0.7 times more efficient than the corresponding values obtained in the Lyapunov case (sample controller). Simulation results for the Jiji earthquake also show an increase in RMS acceleration in both directions for the ARB–FLC case. For better comparison the performance values are plotted

DOI: 10.1002/stc

Table V. Performance indices, RMS values (FN-X and FP-Y).

PI	Control	Newhall	Sylmar	El-Centro	Rinaldi	Kobe	Jiji	Erzinkan
J_7	Lyapunov	0.5600	0.5900	0.8900	0.7900	0.6200	0.6800	0.5100
	FRB–FLC	0.6277	0.6999	0.8765	0.8495	0.7020	0.7244	0.7113
	ARB–FLC	0.5906	0.5875	0.8930	0.7770	0.5662	0.5562	0.5055
J_8	Lyapunov	1.3100	1.1900	1.2900	1.8500	1.3600	1.1300	1.0600
	FRB–FLC	1.2459	1.0983	1.4204	1.7094	1.3704	1.2413	1.1198
	ARB–FLC	1.3896	1.0343	1.3798	1.5365	1.3774	1.4659	0.9906
J_9	Lyapunov	0.4400	0.4700	0.4200	0.4400	0.4200	0.3400	0.4800
	FRB–FLC	0.4246	0.4356	0.4819	0.4161	0.4203	0.3729	0.5111
	ARB–FLC	0.4010	0.3286	0.5033	0.4298	0.3565	0.3450	0.4196

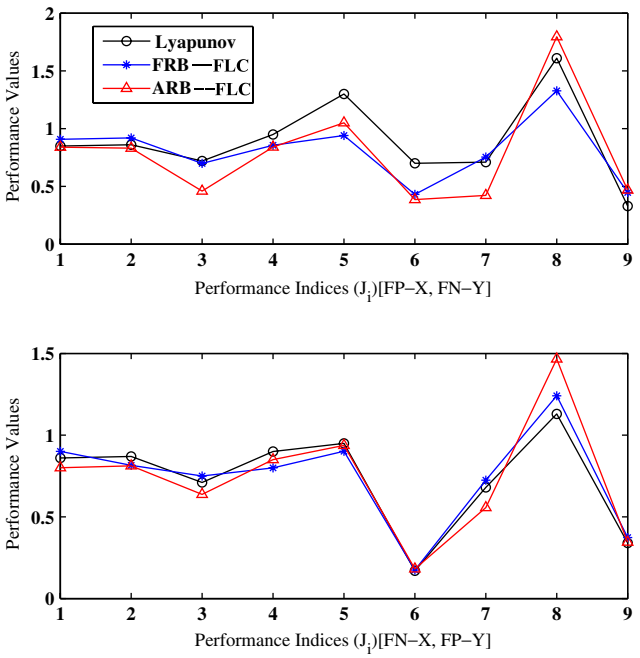

Figure 9. Comparison of performance values [Jiji EQ] for different control schemes.

against performance indices for the Jiji earthquake and are shown in Figure 9. One should observe from the figure (Figure 9) that the performance of FRB–FLC is comparable to ARB–FLC and in many aspects better than the Lyapunov controller. Comparable performance of the FRB–FLC is possible as the base-isolated building acts as a single degree-of-freedom system and the FRB taken is optimal for a single degree-of-freedom as its input–output relationship is based on the first mode of vibration of a structure.

The base displacements at the center of mass of the base for Lyapunov, FRB–FLC, ARB–FLC controllers under the Kobe earthquake are shown in Figure 10 [both the *X*- and the *Y*-directions]. ARB–FLC shows the lowest displacement at the mass center of the base, whereas

DOI: 10.1002/stc

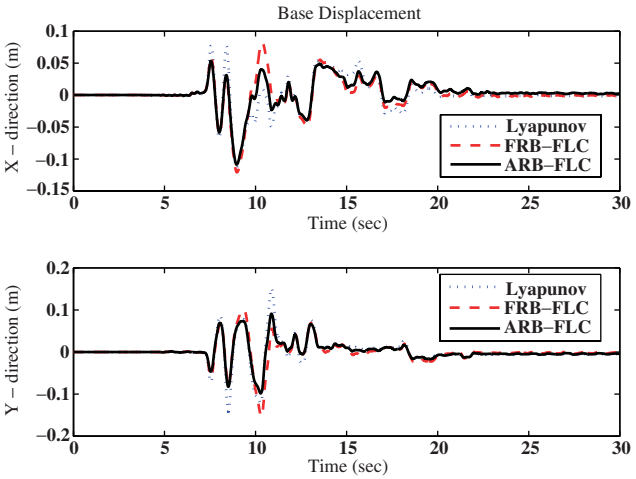

Figure 10. Displacement at the center of mass of the base [Kobe EQ (FP-X, FN-Y)] for different control schemes.

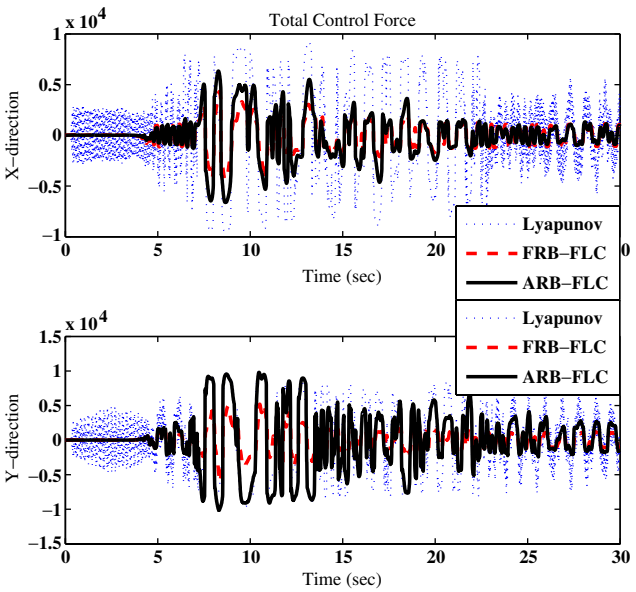

Figure 11. Total control force [Kobe EQ (FP-X, FN-Y)] for different control schemes.

FRB–FLC shows the highest in the *X*-direction and Lyapunov in the *Y*-direction. The total MR damper force required to control the base-isolated building is shown in Figure 11. The controller force in the Lyapunov case has considerable fluctuation from the beginning of the excitation and continues till the end of the excitation. Both FRB–FLC and ARB–FLC show no such fluctuation. The reason for this is that the Lyapunov controller switches the MR damper

DOI: 10.1002/stc

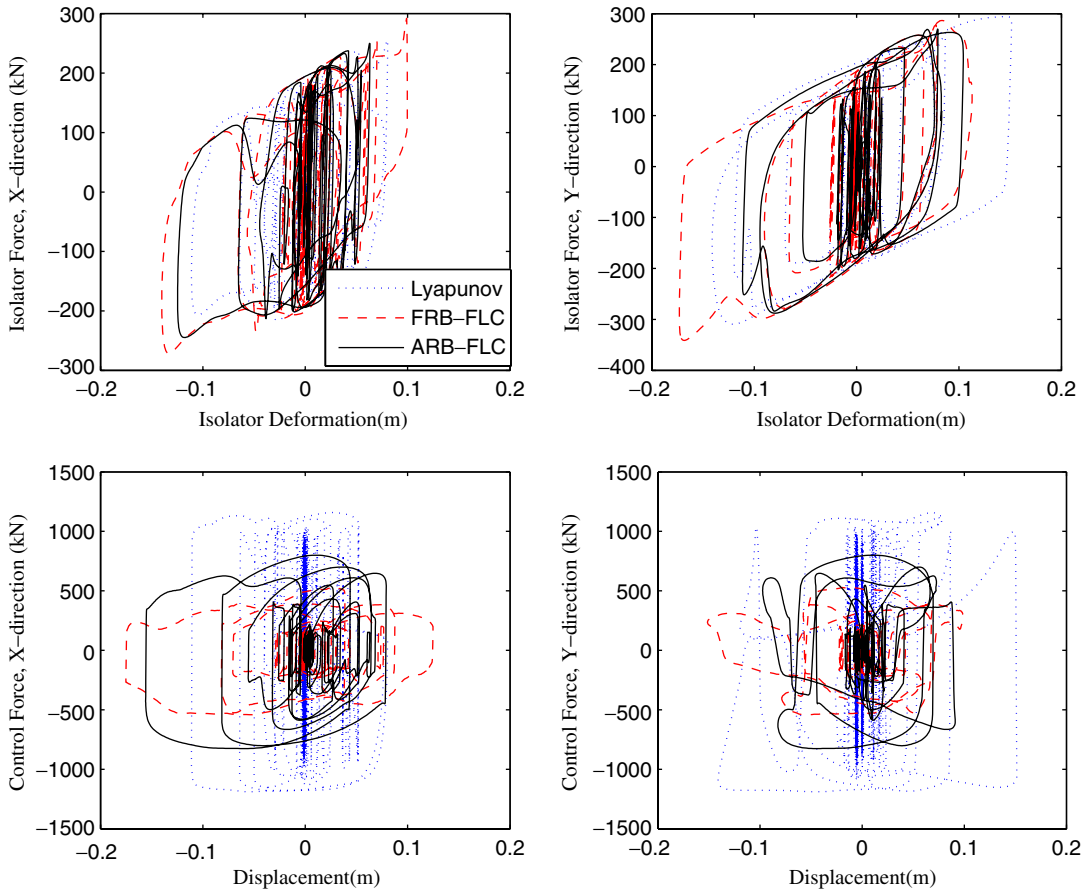

Figure 12. Force displacement loops [Kobe EQ (FP-X, FN-Y)] for different control schemes.

voltage between its minimum and maximum voltage values; therefore, the controller force also fluctuates a lot. In case of the FLC (both FRB and ARB) the voltage change in the MR damper is gradual and therefore such fluctuations do not arise. FRB–FLC demands less controller force and more bearing displacement (see Figure 10) when compared with that of ARB–FLC. However, both FLCs use less controller force than the Lyapunov controller. Figure 12 shows the hysteretic force–displacement loops for the isolator and the MR damper located near the center of mass of the building at the base.

To see the effect of different optimization cost functions on the performance of the controller, another objective function taking into account the controller force in the previous objective function (Equation (3)) has been defined. Therefore, the new objective function can be stated as

$$\phi_2 = w_1\left(\frac{|V_0(t)|}{|\hat{V}_0(t)|-1}\right) + w_2\left(\frac{|x_b(t)|}{|\hat{x}_b(t)|}\right) + w_3\left(\frac{f_{max}|a_f(t)|}{f_{max}|\hat{a}_f(t)|-1}\right) + w_4\frac{|f_d(t)|}{|V_0(t)|} \tag{4}$$

where w_i $(i = 1, 2, 3)$ has the same value as in Equation (3), and $w_4 = 1$. Results are plotted against the ARB with the objective function given in Equation (3) and are shown in Figure 13.

DOI: 10.1002/stc

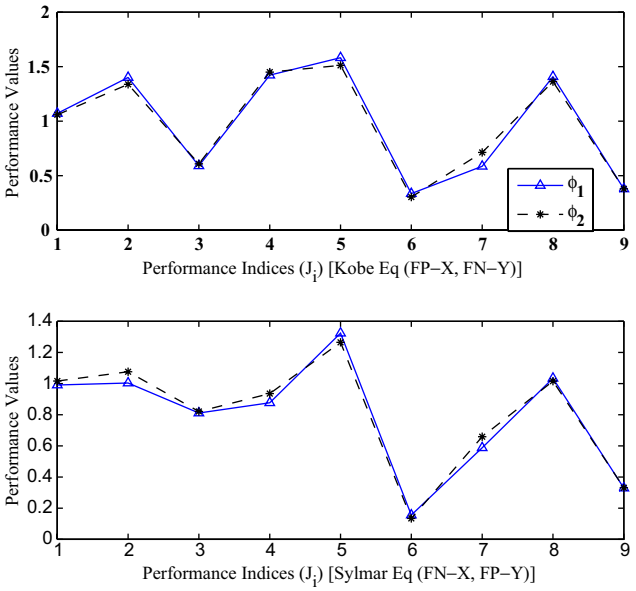

Figure 13. Comparison of J_i for different objective functions [ϕ_1 = without control objective, ϕ_2 = with control objective].

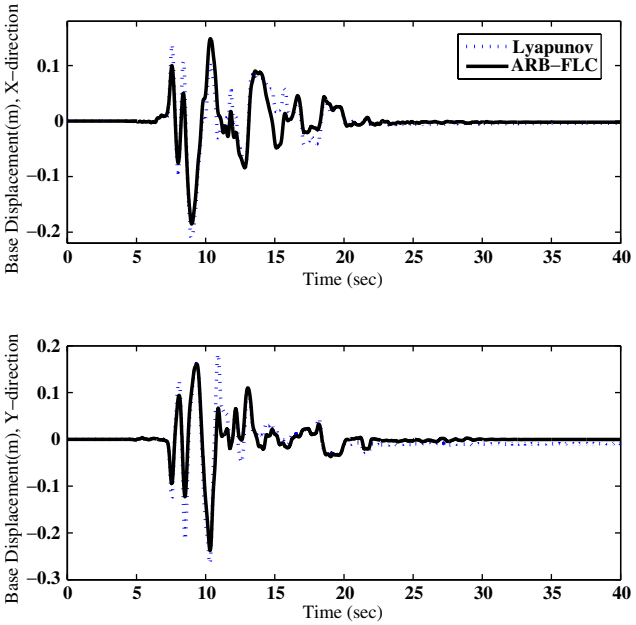

Figure 14. Stability test (scaled up earthquake): displacement at the center of mass of the base [Kobe EQ (FP-X, FN-Y)].

DOI: 10.1002/stc

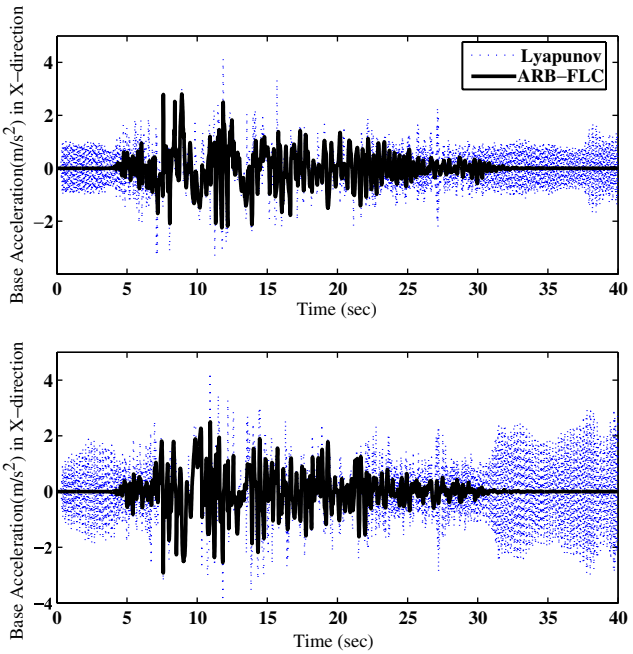

Figure 15. Stability test (scaled up earthquake): acceleration at the center of mass of the base [Kobe EQ (FP-X, FN-Y)].

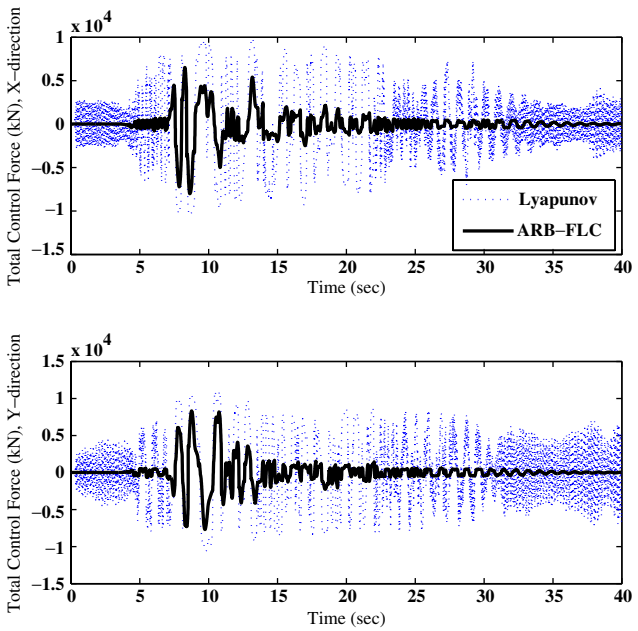

Figure 16. Stability test (scaled up earthquake): total control force [Kobe EQ (FP-X, FN-Y)].

DOI: 10.1002/stc

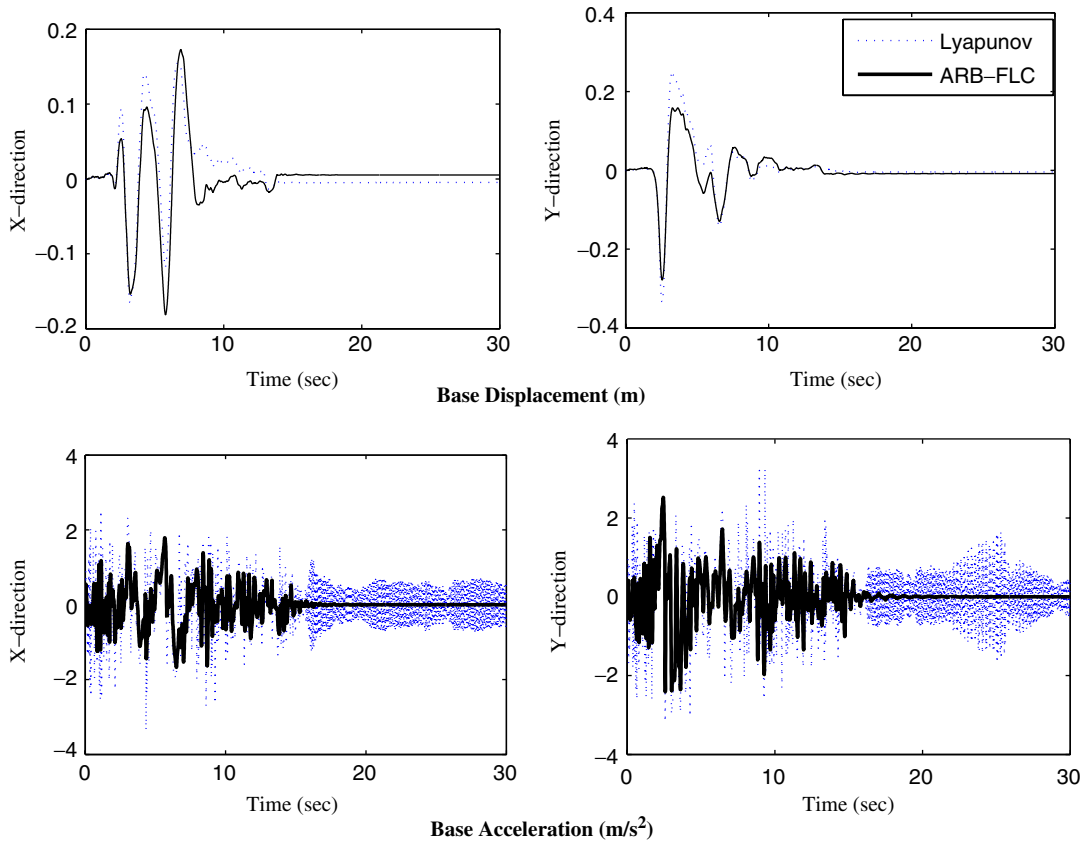

Figure 17. Stability test (scaled up mass): base displacement and acceleration [Rinaldi EQ (FP-X, FN-Y)].

In Figure 13, ϕ_1 and ϕ_2 are referred to as the objective functions in Equations (3) and (4), respectively. No significant change is observed but the peak control force required (J_6) is less and at the same time the bearing displacement is increased slightly in the ϕ_2 case.

5.1. Stability of ARB–FLC

Only few methods are available that guarantee or check the stability of fuzzy controllers [8]. Validation of stability is performed with simulations and tests to check whether the controller system returns at rest from initial conditions that were caused by the external disturbance. In practice one simulates the closed-loop system with the state variables that seem to show the worst response. The test consists of checking the ability of the controller to reduce the response and to drive the system to the rest position after the initial transient phase. In this paper stability tests have been performed considering scaled up [1.5 times] input earthquake excitations. To assess the stability of the system, free vibration of the system for an additional 10 s after the earthquake excitation is over has been carried out. The stability check has been performed for all earthquake records and for the Lyapunov controller and ARB–FLC. The response plots

DOI: 10.1002/stc

have been shown for the Kobe earthquake [Figures 14–16]. Figure 14 shows the displacement time history at the center of mass of the building at the base. It is evident from the figure (Figure 14) that both the controllers are effective in bringing down the base displacement to rest within the time [10 s]. However, it has been observed from the acceleration time histories (Figure 15) that the acceleration in case ARB–FLC dies down fast; the Lyapunov controller, on the contrary, does not show a slow down of acceleration, rather it shows an increase in acceleration. The same nature of time history has been observed in the case of total control force (Figure 16). The reason can be attributed to the switch of the MR damper voltage from minimum to maximum values and the sluggish nature of the robust Lyapunov controller.

To observe the behavior of ARB–FLC under parameter variation, total mass at the base has been increased by 20% times keeping all other parameters fixed and then the simulation has been run. The acceleration response at the base center of the building for the Rinaldi earthquake has been shown in Figure 17. It is evident from Figures 14 to 17 that the performance of the ARB–FLC controller is superior to that of the Lyapunov controller in reducing the building responses and bringing down the responses to rest within minimal time for parameter uncertainity (scaled up earthquake time history and structure mass).

6. CONCLUSION

A GA-optimized FLC strategy with a variable rule base has been developed for the base-isolated nonlinear benchmark building problem. MR dampers have been used as controllers. Effectiveness of the FLC-based semi-active MR damper has been demonstrated for the base-isolated building benchmark problem. Performance of the proposed control system has been found to be better than the sample control strategy provided with the benchmark definition. A number of sensors and actuators have been kept same as that of the benchmark exercise problem. The ARB–FLC provides the damper voltage as an output. Unlike the clipped optimal technique the ARB–FLC-driven MR damper voltage can take any value between [0,1], which not only provides added robustness to the closed-loop system, but also uses reduced peak control force. Two optimal FLCs have been proposed, optimized online at every simulation time step. The variable rule base has been designed based on a geometric approach and therefore has less computational overhead. The variable rule base maintains a symmetry in the input–output space pattern and therefore assures stability. The stability test of the ARB–FLC has also been shown with increased earthquake magnitude and increased mass. To show the efficiency of ARB–FLC, simulations with FRB–FLC have been done and compared with ARB–FLC and the sample control technique provided with the benchmark exercise. A multi-objective cost function with fixed weights has been used in this study.

REFERENCES

1. Spencer B, Nagarajaiah S. State of the art of structural control. *Journal of Structural Engineering—ASCE* 2003; **129**:845–856.
2. Narashiman S, Nagarajaiah S. Smart base isolated buildings with variable friction systems: H_∞ controller and novel SAIVF device. *Earthquake Engineering and Structural Dynamics* 2006; **35**:920–942.
3. Soong T, Spencer B. Supplemental energy dissipation: state of the art and state of the practice. *Engineering Structures* 2002; **24**:243–259.

DOI: 10.1002/stc

4. Ghaboussi J, Joghataie A. Active control of structures using neural networks. *Journal of Engineering Mechanics—ASCE* 1995; **121**:555–567.
5. Bani-Hani K, Ghaboussi J. Nonlinear structural control using neural networks. *Journal of Engineering Mechanics—ASCE* 1998; **124**:319–327.
6. Joghataie A, Ghaboussi J. Neural network and fuzzy logic in structural control. *Proceedings of the First World Conference on Structural Control*, Los Angeles, CA, 1994; WP1:21–30.
7. Subramaniam R, Reinhorn A, Riley M, Nagarajaiah S. Hybrid control of structures using fuzzy logic. *Microcomputer and Civil Engineering* 1996; **11**:1–17.
8. Battaini M, Casciati F, Faravelli L. Fuzzy control of structural vibration: an active mass system driven by fuzzy controller. *Earthquake Engineering and Structural Dynamics* 1998; **27**:1267–1276.
9. Ali SF, Ramaswamy A. Developments in structural optimization and applications to intelligent structural vibration control. In *Intelligent Computational Paradigms in Earthquake Engineering*, Lagaros N, Tsompanakis Y (eds). Idea Group Publishing: New York, 2007; 101–121.
10. Ahlawat A, Ramaswamy A. Multiobjective optimal absorber system for torsionally coupled seismically excited structures. *Engineering Structures* 2003; **25**:941–950.
11. Ahlawat A, Ramaswamy A. Multiobjective optimal fuzzy logic controller driven active and hybrid control systems for seismically excited nonlinear buildings. *Journal of Engineering Mechanics—ASCE* 2004; **130**:416–423.
12. Jang J, Sun C, Mizutani E. *Neuro Fuzzy and Soft Computing*. Pearson Education: India, 2005.
13. Ali SF, Ramaswamy A. FLC based semi-active control of buildings using magneto-rheological dampers. *Proceedings of the 2nd International Congress on Computational Mechanics and Simulation*, Indian Institute of Technology, Guwahati, India, 2006.
14. Wang L, Kazmierski T. VHDL-AMS based genetic optimization of a fuzzy logic controller for automotive active suspension systems. *Proceedings of* 2005 *IEEE International Workshop on Behavioral Modeling and Simulation* 2005; 124–127.
15. Blumel A, Hughes E, White B. Multi-objective evolutionary design of fuzzy autopilot controller. In *Evolutionary Multi-criterion Optimization*, Zitzler E (ed.). Springer: Berlin, 2007; 669–680.
16. Yan G, Zhou LL. Integrated fuzzy logic and genetic algorithms for multi-objective control of structures using MR dampers. *Journal of Sound and Vibration* 2006; **294**:368–382.
17. Dounis A, Tiropanisy P, Syrcos G, Tseles D. Evolutionary fuzzy logic control of base-isolated structures in response to earthquake activity. *Journal of Structural Control and Health Monitoring* 2007; **14**:62–82.
18. Kim HS, Roschke PN. GA-fuzzy control of smart base isolated benchmark building using supervisory control technique. *Advances in Engineering Software* 2007; **38**:453–465.
19. Byrne J. GA-optimization of a fuzzy logic controller. *Masters Thesis*, School of Electronic Engineering, Dublin City University, 2003.
20. Nagarajaiah S, Narashiman S, Johnson E. Phase II smart base isolated benchmark building with nonlinear isolation systems. *Proceedings of 4th World Conference on Structural Control and Monitoring*, San Diego, CA, 2006.
21. Narashiman S, Nagarajaiah S, Johnson E, Gavin H. Smart base isolated benchmark building part I: problem definition. *Journal of Structural Control and Health Monitoring* 2006; **13**:573–588.
22. Nagarajaiah S, Narasimhan S. Smart base isolated benchmark building part II: phase I sample controllers for linear isolation system. *Journal of Structural Control and Health Monitoring* 2006; **13**:589–604.
23. Erkus B, Johnson E. Smart base isolated benchmark building part III: a sample controller for bilinear isolation. *Journal of Structural Control and Health Monitoring* 2006; **13**:605–625.
24. Narashiman S, Nagarajaiah S, Johnson E. Smart base isolated benchmark building Part IV: phase II sample controllers for nonlinear isolation systems. *Journal of Structural Control and Health Monitoring* 2008. DOI: 10.1002/stc.267.
25. Shi Y, Eberhart R, Chen Y. Implementation of evolutionary fuzzy systems. *IEEE Transactions on Fuzzy Systems* 1999; **7**(2):109–119.
26. Casciati F, Faravelli L, Yao T. Control of nonlinear structures using the fuzzy control approach. *Nonlinear Dynamics* 1996; **11**:171–187.
27. MATLAB®. The software for numerical computing, version 7.0.1 (R14). *The MathWorks*, 2004.
28. Cordon O, Herrera F, Hoffmann F, Magdalena L, Gomide F. Ten years of genetic fuzzy systems: current framework and trends. *Fuzzy Sets and Systems* 2004; **141**:5–31.
29. Driankov D, Hellendoorn H, Reinfrank M. *An Introduction to Fuzzy Control*. Narosa Publishing House: Kolkata, 1992.
30. Krishnakumar K. Microgenetic algorithms for stationary and nonstationary function optimization. In *Proceedings of SPIE Intelligent Control and Adaptive Systems*, Rodriguez G (ed.), vol. 1196, 1989; 289–296.
31. Goldberg D. Sizing populations for serial and parallel genetic algorithms. *Proceedings of the 3rd International Conference on Genetic Algorithms*, 1989.
32. Pulido GT, Coello CAC. The micro genetic algorithm 2: towards online adaptation in evolutionary multiobjective optimization. In *Evolutionary Multi-criterion Optimization*, Fonseca C, Fleming P, Zitzler E, Deb K, Thiele L (eds). Springer: Berlin, 2003; 252–266.

33. Haupt R, Haupt S. *Practial Genetic Algorithm* (2nd edn). Wiley/Interscience: New York, 2004.
34. Chipperfield A, Fleming P, Pohlheim H, Fonseca C. Genetic algorithm toolbox: for use with matlab. ver-1.2, *Automatic Control Systems Engineering*, University of Sheffield, 2006. Available at http://www.shef.ac.uk/acse/research/ecrg/getgat.html.
35. Baker J. Reducing bias and inefficiency in the selection algorithm. *Proceedings of the Second International Conference on Genetic Algorithms and their Application*, Hillsdale, 1987; 14–21.
36. Scott SD, Samal A, Seth S. HGA: a hardware-based genetic algorithm. *Proceedings of the 1995 ACM Third International Symposium on Field-Programmable Gate Arrays*, Montessy, CA, U.S.A., 1995; 53–59. ISBN: 0-89791-743-X.
37. Chen SD, Chen PY, Wang YM. A flexible genetic algorithm chip, 2006. Available from http://140.134.132.124:8080/dspace/handle/2377/506.
38. Rahman MA, Uddin MN. A novel genetic algorithm based fuzzy logic controller for IPM synchronous motor drive. *IEEE International Symposium on Industrial Electronics*, Rio de Janeiro, Brazil, ISIE-03, 2003; 2:1007–2:1010.
39. Al-Osaimi SA, Abdennour A, Al-Sulaiman AA. Hardware implementation of a fuzzy logic stabilizer on a laboratory scale power system. *Electric Power Systems Research* 2005; **74**:9–15.
40. Shook D, Lin PY, Lin TK, Roschke PN. A comparative study in the semi-active control of isolated structures. *Smart Materials and Structures* 2007; **16**:1433–1446.
41. Hailin J, Dongming J. Self-adaptation of fuzzy controller optimized by hardware-based GA. *Proceedings of the 6th International Conference on Solid-State and Integrated-Circuit Technology* (*IEEE*), vol. 2, 2001; 1147–1150.
42. Tan K, Lee T, Khor E, Ang D. Design and real-time implementation of a multivariable gyro-mirror line-of-sight stabilization platform. *Fuzzy Sets and Systems* 2002; **128**:81–93.

DOI: 10.1002/stc